

1 **A dedicated robust instrument for water vapor generation at low-humidity for use with a laser water**
2 **isotope analyzer in cold and dry polar regions.**

3
4 Christophe Leroy-Dos Santos¹, Mathieu Casado^{1,2}, Frédéric Prié¹, Olivier Jossoud¹, Erik Kerstel³, Morgane
5 Farradèche¹, Samir Kassi³, Elise Fourré¹, Amaëlle Landais^{1,*}

6
7 ¹ Laboratoire des Sciences du Climat et de l'Environnement, CEA-CNRS-UVSQ-Paris Saclay-IPSL, Gif-sur-
8 Yvette, France

9 ² Alfred Wegener Institut, Helmholtz Center for Polar and Marine Research, Potsdam, Germany

10 ³ Laboratoire Interdisciplinaire de Physique, CNRS - Université Grenoble Alpes, Grenoble, France

11 * corresponding author: amaelle.landais@lsce.ipsl.fr

12

13 **Abstract**

14 Obtaining precise continuous measurements of water vapor isotopic composition in dry places (polar or
15 high-altitude regions) is an important challenge. The current limitation is the strong influence of humidity
16 on the measured water isotopic composition by laser spectroscopy instruments for low-humidity levels
17 (below 3,000 ppmv). This problem is addressed by determining the relationships between humidity and
18 measured $\delta^{18}\text{O}$ and δD of known water standards. We present here the development of a robust field
19 instrument able to generate water vapor, down to 70 ppmv, at very stable humidity levels (average 1σ
20 lower than 10 ppmv). This instrument, operated by a Raspberry interface, can be coupled to a commercial
21 laser spectroscopy instrument. We checked the stability of the system as well as its accuracy when
22 expressing the measured isotopic composition of water vapor on the VSMOW-VSLAP scale. It proved to
23 be highly stable during autonomous operation over more than one year at the East Antarctic Concordia
24 and Dumont d'Urville stations.

25

26

27 **1. Introduction**

28 The recent development of laser spectroscopy instruments now enables the continuous measurement of
29 the isotopic composition of water vapor at many observation stations all around the world (Bailey et al.,
30 2015; Bastrikov et al., 2014; Schmidt et al., 2010; Sodemann et al., 2017; Tremoy et al., 2011). In particular,
31 the isotopic composition of the water vapor has proven to be a very useful tool to document moist synoptic
32 events in many locations (Bonne et al., 2014; Guilpart et al., 2017). In polar regions, the water vapor
33 isotopic signal is not only useful to detect the origin of moist air (Bréant et al., 2019; Kopec et al., 2014)
34 but also to improve the interpretation of the isotopic composition of water in surface snow and ice core
35 archives (Steen-Larsen et al., 2014). Indeed, exchanges are occurring after deposition between the surface

36 snow and the water vapor leading to modifications of the isotopic composition of the former and hence
37 of the archived ice (Casado et al., 2016, 2018; Ritter et al., 2016).

38 Obtaining continuous and accurate measurements of the water vapor isotopic composition expressed on
39 the VSMOW-VSLAP scale measurements of the water vapor isotopic composition at Concordia station in
40 central Antarctica is a key scientific challenge since the deep ice core drilled there, EPICA Dome C, provides
41 the oldest continuous water isotopic record expressed on the VSMOW-VSLAP scale to date (Jouzel et al.,
42 2007). It is thus a key reference for the study of past climate, and a correct interpretation of the isotopic
43 record relies on the quantification of the transfer function between climate parameters and water isotopic
44 composition in ice, itself influenced by exchanges with water vapor in the upper layers of the firn (Casado
45 et al., 2018). Such knowledge is also of uttermost importance for the interpretation of water isotope
46 records from the starting deep drilling project “Beyond EPICA-Oldest Ice” (<https://www.beyondepica.eu>),
47 whose aim is to drill a 1.5-million-year old ice core at the Little Dome C site located 40 km away from
48 Concordia station, hence with similar low temperature and humidity conditions.

49 One of the main limitations of the current commercial instruments when deployed in polar regions is their
50 relatively poor performance at low water vapor concentration. Generally, the precision of the measured
51 isotopic ratios $\delta^{18}\text{O}$ and δD rapidly worsens when the water mixing ratio decreases to humidity levels
52 below 3,000-5,000 ppmv (part-per-million per volume) (Bonne et al., 2014; Weng et al., 2020). However,
53 in remote continental areas in Greenland and Antarctica, temperatures in winter can drop to very low
54 values, leading to humidity levels down to 10 ppmv (Genthon et al., 2017). Arguably one of the most
55 extreme experiments for continuous measurement of the water vapor isotopic composition was the
56 deployment of a commercial Picarro L2130-i instrument at the East Antarctic French-Italian station of
57 Concordia where the mean annual temperature is around -54°C and the humidity barely exceeds 1,000
58 ppmv during the warmest summer days (Casado et al., 2016). For such applications, there are two major
59 impacts of low-humidity on the raw isotopic signal: first, we generally observe an apparent increase in the
60 $\delta^{18}\text{O}$ and δD with decreasing humidity level and second, the standard deviation associated with the
61 continuous measurements of $\delta^{18}\text{O}$ and δD of the water vapor increases. This can lead to overall
62 uncertainties of several ‰ for $\delta^{18}\text{O}$ and tens of ‰ for δD . It is thus of uttermost importance to have a
63 correct determination of the humidity dependency of the water vapor isotopic ratios.

64 Commercial instruments from Picarro Inc. are usually associated with a Picarro Standard Delivery Module
65 (SDM) designed to generate humidity at stable levels between 5,000 and 30,000 ppmv. Using such a set-
66 up for humidity levels below 5,000 ppmv leads to large uncertainties in the determination of the humidity
67 influence on the water vapor isotopic composition (e.g. Guilpart et al., 2017). These uncertainties are due
68 both to the instability of the water vapor generation using the SDM (in terms of water concentration –
69 humidity – and/or isotopic composition) and to the analytical noise in the spectroscopy measurements
70 when the absorption signals are weak. An alternative commercial device is the LGR (Los Gatos Research)

71 calibration system (Water Vapor Isotope Standard Source, WVISS), which uses a nebulizer to
72 instantaneously evaporate micro-droplets of liquid water from a standard reservoir into a large (1 L)
73 vaporizing chamber (Dong and Baer, 2010). This system is very stable and well adapted for a humidity
74 range between 2,500 and 25,000 ppmv (Aemisegger et al., 2012).

75 Several home-made water vapor injection systems have been developed with the specific aim to achieve
76 a better stability of the generated humidity at low-humidity levels. A first approach is to use a dew point
77 generator injecting small amounts of water into dry air (Lee et al., 2005; Wang et al., 2009). This approach
78 is time consuming as it takes long to reach equilibrium and relies on a very precise knowledge of the
79 temperature to quantify the isotopic fractionation. A method using a piezoelectric microdroplet generator
80 into a dry air stream could generate water mixing ratios between 12 and 3,500 ppmv (Iannone et al., 2009;
81 Sturm and Knohl, 2009; Sayres et al., 2009). However, adjustment of humidity level and long-term stability
82 were difficult to obtain with such devices. Systems relying on the use of syringe pumps were also built by
83 Gkinis et al. (2010) and Tremoy et al. (2011): a small fraction of the input stream of liquid water is
84 introduced into a hot oven where water is vaporized in the presence of a dry air flow. These systems cover
85 humidity range between 2,000 and 30,000 ppmv. Finally, bubbler systems, in which dry air flows through
86 a large volume of water to create saturated vapor, are very robust but can only produce water vapor at
87 high-humidity levels (Ellehoj et al., 2013). The aforementioned devices are unfortunately not well suited
88 for automatic long-term operation at low-humidity levels. During the 2014-2015 summer field season at
89 Concordia station in Antarctica, a home-made humidity generator specifically designed for low-humidity
90 levels (Landsberg, 2014) has been deployed (Casado et al., 2016). The device used dual high-precision,
91 low-volume, syringe pumps to generate stable humidity levels at two different isotopic compositions over
92 the range from 100 to 800 ppmv (Casado et al., 2016). Unfortunately, we observed quite a large scattering
93 among the isotopic values measured at similar humidity levels, as well as a large discrepancy between the
94 humidity dependency of the water isotopic ratios measured in the field and the one measured in the
95 laboratory. Upon return to the laboratory, these defaults were traced primarily to tiny leaks in the water
96 supply lines to the syringes.

97 Therefore, we re-engineered the prototype by Landsberg (2014) in order to develop a robust and
98 autonomous device for stable low-level humidity generation for the purpose of precise humidity
99 calibration of spectroscopic instruments. Such devices have now been operating with minimum manual
100 intervention for more than one year at two polar stations in Antarctica, Dumont d'Urville and Concordia,
101 coupled to Picarro laser spectroscopy instruments. We detail here the technical description of the
102 instrument and show key performance characteristics, enabling, for instance, a discussion of small
103 amplitude signals such as the diurnal variability of the water vapor isotopic composition in remote dry
104 sites in East Antarctica.

105

2. New vapor generator for low-humidity levels

The low-humidity level generator (LHLG) developed here relies on the same principle as the one developed by Landsberg (2014), i.e., a steady, undersaturated evaporation of a liquid water droplet at the tip of a needle into a dry air stream inside a small evaporation chamber. Based on this first prototype, the instrument has been remodeled including a specific hardware and software design.

2-1-Physical principle

The LHLG is based on undersaturated evaporation of a small droplet at the tip of a needle (Figure 1). Liquid water is pushed through a needle around which dry air is flowing. Dry air is obtained from a bottle of high purity synthetic air with pressure regulation through two manometers connected in series. The mass flux of water f_L is kept low compared to the air mass flow f_A so that the relative humidity RH of the downstream moist air flow remains low ($RH < 0.1$). Therefore, the air stays largely undersaturated and its humidity is controlled only by the flow of liquid water in the needle and that of the dry air upstream of it. The mixing ratio (or humidity) of the air as classically provided by a Picarro instrument is given by:

$$MR = \frac{d_{H_2O} \times f_L \times R \times T_{st}}{f_A \times P_{st} \times M_{H_2O}} \quad (\text{eq. 1})$$

where $d_{H_2O} = 1000 \text{ kg m}^{-3}$ is the density of water, $R = 8.314 \text{ J mol}^{-1} \text{ K}^{-1}$ is the universal gas constant, $T_{st} = 293.15 \text{ K}$ and $P_{st} = 1013.25 \text{ hPa}$ are standard conditions of temperature and pressure and $M_{H_2O} = 18.10^{-3} \text{ kg mol}^{-1}$.

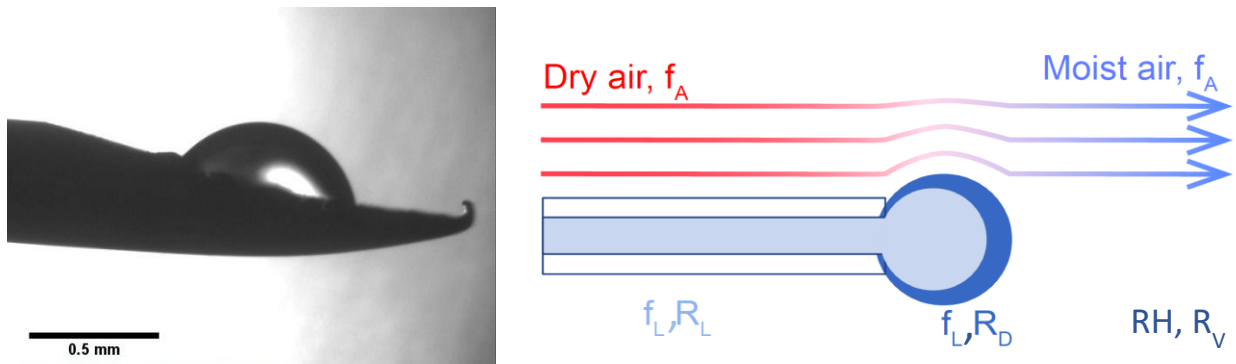


Figure 1: Evaporation of a droplet in the humidity generator chamber: left, picture from the prototype from Landsberg (2014); right, schematics of the water molecules being transferred to the air flow (Casado, 2016).

Physically, when the flux of water or air is changed, there is first a transient regime during which the radius

133 of the droplet changes, modifying the evaporative surface and therefore the humidity of the outgoing air.
134 Once a stationary regime is reached, the radius of the droplet is stabilized and the humidity is given by
135 equation 1. In this regime, there is no accumulation of water molecules in the system and therefore the
136 isotopic composition of the vapor produced is equal to the isotopic composition of the liquid water
137 injected in the needle: $R_v = R_L$ (note that because of the fractionation during the transition phase, the
138 isotopic composition of the droplet R_D is different from R_L and R_v , see Kerstel, 2020). When changing the
139 flux of evaporating water, we modify the size of the evaporating surface and therefore the radius of the
140 drop. The evolution of the radius of the drop can be obtained from the resolution of a non-linear
141 differential equation of the volume V of the drop:

$$142 \quad dV/dt = f_L - f_{evap} \quad (\text{eq. 2})$$

143 where $f_{evap} = k_e \times S$ is the evaporation flux depending of k_e , the evaporation rate, and S , the surface area of
144 the drop exposed to the dry air. A good approximation is to consider the shape of the drop as a fraction of
145 a sphere of variable radius intercepted by the surface of a disk of constant radius (the syringe tip). By
146 solving numerically the differential equation (2), it is possible to faithfully simulate the behavior of the
147 device under changing conditions (Kerstel, 2020). This numerical approach validates the theoretical
148 explanation of the undersaturated evaporation of the droplet. Importantly, it is noted that in steady-state
149 as is the case for our application, the isotopic composition of the generated humid air is identical to that
150 of the injected water stream, and therefore does not depend on the infusion rate, nor on the specific
151 humidity.

152 **2-2- Instrument conception**

153 **- Technical realization**

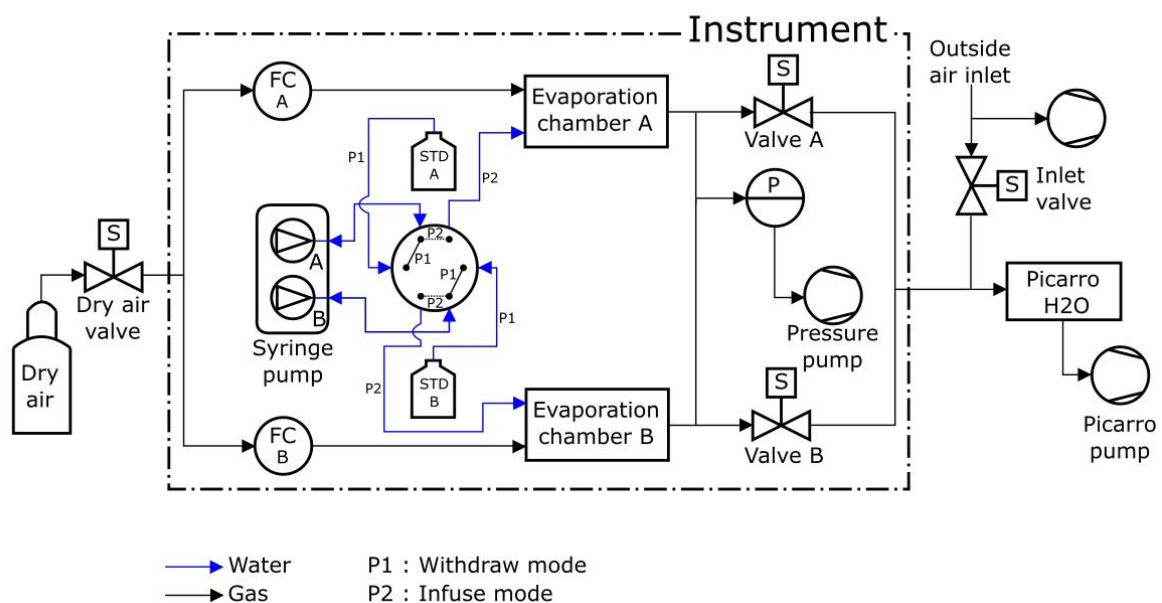
154 As the LHLG relies on operating in a stationary regime, it is important that the dry air input and the water
155 input are steady. Thus, the air and water fluxes, as well as the air pressure in the evaporation chamber are
156 controlled by electronic PID regulators. Temperature intervenes through its effect on fractionation and
157 the evaporation rate (apart from a negligible effect on the flow controller stability), which could lead to a
158 departure from steady-state operation. For these reasons, the temperature of the evaporation chambers
159 was maintained at 20°C (within 1°C over 24 hours).

160 The dry air flux is regulated by a high-precision mass flow controller (Vögtlin GSC-A9TS-DD22), that has an
161 operating range from 6 to 600 sccm ($\text{std cm}^3 \text{ min}^{-1}$) and an accuracy of 3.3 sccm. The water flux is regulated
162 by a high-precision syringe pump (Harvard Apparatus Pump 11 Pico Plus Elite Dual), which can produce a
163 water flow down to 10.8 pL min^{-1} with an accuracy of 0.35 % using syringes with a volume ranging from
164

168 10 μL to 250 μL . We operate in the routine mode with a dry air flow of 300 sccm and a water flow between
 169 0.02 to 0.5 $\mu\text{L min}^{-1}$ using mainly 50 or 100 μL syringes. A syringe pump is equipped with two syringes that
 170 provide two water flows into two evaporation chambers in parallel (Figure 2). Each syringe is connected
 171 to a water reservoir and to an evaporation chamber by a double 3-way liquid valve (Rheodyne MXX777603)
 172 switching from an “infuse” mode to a “withdraw” mode to refill the syringes. The water in the water
 173 reservoirs is sampled every month to check its isotopic composition and renewed when the level of water
 174 is below half the maximum level. A maximum evolution of the isotopic composition of the lab-standard
 175 filling the water reservoirs has been observed as 0.05‰ and 0.5‰ respectively for $\delta^{18}\text{O}$ and δD over a 2-
 176 month period.

177 A major change to the instrument designed by Landsberg (2014) is the introduction of the double 3-way
 178 valve with leak-tight connections and an internal volume of 1.9 μL . This modification is an important
 179 improvement as it enables automatic handling of the lab-standards from a reservoir to the evaporation
 180 chamber with a robust connection, avoiding in particular potential air bubbles in the water flow. Indeed,
 181 the compressibility of air bubbles trapped in the water flow can lead to flow irregularities by amplification
 182 of small non-linearities in the progression of the syringe plunger. This would lead to non-steady state
 183 operation, which in turn would create artefacts in the humidity and isotopic composition, reducing the
 184 performance of the calibration device (see Kerstel 2020). In addition, the 3-way valve provides the
 185 opportunity of a “withdrawn” mode in which the syringes draw lab-standard water from a reservoir. When
 186 equipped with 100- μL syringes, the instrument can operate for several hours up to one day between refills.
 187 With the addition of the auto-refill option and the effective suppression of bubbles, the instrument can be
 188 used unattended for many months, as required for an Antarctic winter field campaign.

189



190

191 **Figure 2:** Humidity generator schematic diagram (see supplementary Table S1 for details on the different
192 elements)

193
194 The evaporation chambers are stainless steel cylinders equipped with specific connectors (Swagelok Ultra-
195 Torr SS-4CD-TW-25) holding silicon rubber septa through which needles are inserted toward the middle of
196 the chamber. The pressure in both chambers is regulated by a pressure controller (Bronkhorst P-702CV-
197 1K1A-AAD-22-V) with a precision of 3 mbar in a range from 0 to 1,000 mbar. This pressurization of the two
198 chambers combined with the relatively high flow (higher than required by the infrared spectrometers)
199 enables maintaining a steady state whether or not the infrared spectrometer is connected, and increases
200 the time efficiency of calibration procedures. The spectrometer is not sensitive to the inlet pressure, the
201 precision of the pressure controller is not an essential aspect. On the contrary, the precision of the flow
202 controller is key for the precision of the humidity level produced by the instrument: it is of 1% for the air
203 flow which is comparable to the precision of the measurement of the humidity level with the optical
204 spectrometer. When the instrument is connected to the infrared spectrometer, the excess humid air flow
205 is exhausted to the room through the pressure pump and the spectrometer only pumps what is required
206 (Figure 2).

207 The control of the instrument is ensured by a Raspberry Pi that can be interfaced to a Picarro water
208 analyzer (L2130-i in our case) in sequencer mode (see below). The hardware has been designed to meet
209 the specifications dictated by field conditions: 1) All components are fixed in a transportable case (except
210 the dry air bottle), isolated from vibration by an anti-vibration foam. 2) A panel of connectors (HDMI, USB,
211 Ethernet, etc.) ensures the accessibility to the instrument when it is closed. 3) The electrical and electronic
212 parts (e.g. power supply, Raspberry Pi) are separated from the rest of the instrument (e.g. sensors, gauges).
213 Both the electrical and electronic parts are fully and easily accessible in case of failure.

214

215 - **Software details**

216 The control software has been developed using open source Python libraries and homemade drivers,
217 including a user interface displaying the state of relevant components and the value of the different
218 sensors. The software (HumGen) can be downloaded on line (<https://github.com/ojsd/humgen>;
219 <https://doi.org/10.5281/zenodo.4003465>).

220 The LHLG can operate in eight different states, each state representing a specific setup for each element
221 (valves position, syringe pump infusion rate, dry air flow rate, pressure). Those eight states can be divided
222 into three categories: a routine mode, an expert mode and a humidity dependence calibration mode. The
223 simple mode is composed of six predefined states referring to the classic isotopic calibration in everyday
224 routine operation (Table 1): 1) measurement of the outside air water vapor isotopic composition; 2) drying
225 of the cavities; 3) “humidity boost”, in order to reach faster the desired humidity level in the cavities; 4)

226 injection of the standard A in the corresponding evaporation chamber at a set humidity level; 5) injection
 227 of the standard B in the corresponding evaporation chamber; 6) refill of the syringes. The expert mode is
 228 useful to adjust each parameter manually: flow rates on the controllers FCA and FCB, opening of the
 229 electrovalves A and B, mode (infuse or withdraw) and infused rate for the syringe pump, pressure
 230 regulation, state of the double three-way valve, activation of the pressure pump at the exhaust, opening
 231 of external electrovalves from the dry air tank and to the inlet (Figure 2). The humidity dependence
 232 calibration mode produces a scale of increasing humidity steps in the evaporation chambers (e.g. from 100
 233 ppmv to 1000 ppmv, through steps of 100 ppmv for 50 minutes for each standard). The details of the
 234 sequence (standard type, humidity level and duration of each step) is defined in a text file by the operator
 235 from the Raspberry interface, the Raspberry being itself connected to Ethernet for remote access.
 236 The Picarro L2130-i analyser has an External Valve Sequencer, which is able to turn on/off up to six
 237 electrovalves and create loop sequences with defined durations for each step of the sequence. This tool
 238 can be diverted from its original purpose by using it as a 6-digit code: each of the humidity generator state
 239 is associated with a code. When the Picarro Valve Sequencer matches one of the state code, this state is
 240 triggered on the humidity generator. This eases both the operator's activities and the data post-treatment,
 241 because the current valve status - thus the calibration instrument state - is saved in the analyzer output
 242 data file, in the "ValveMask" column. The Raspberry inside the LHLG reads the Valve Sequencer state code
 243 using the Picarro's Remote Control Interface (a RS232 serial connection through one of the rear-face DB9
 244 connector).
 245

States (min)	Flow FCA (sccm)	Flow FCB (sccm)	Valve A	Valve B	Syringe Pump ($\mu\text{L}/\text{min}$)	Inlet Valve	Dry air Valve	Pressure controller (mbar)	Pressure Pump for exhaust	Double 3-way valve
Outside air (1100)	0	0	Closed	Closed	0	Open	Closed	Off	Off	To chamber
Drying (20)	400	400	Open	Open	0	Closed	Open	Off	Off	To chamber
Boost (0.7)	300	300	Open	Open	Infuse at 2.5	Closed	Open	905	On	To chamber
Standard A (50)	300	150	Open	Closed	Infuse at 0.25	Closed	Open	905	On	To chamber

Standard B (50)	150	300	Closed	Open	Infuse at 0.25	Closed	Open	905	On	To chamber
Reset (1)	Closed	Closed	Closed	Closed	Withdraw max speed	Open	Closed	Off	Off	From standard

246 **Table 1:** Typical routine sequence of measurements + calibration for two standards A and B at 1000 ppmv
247 for a measurement site located at sea level. No mixing occurs between standards A and B during steps
248 “Standard A” and “Standard B” (see supplementary text S1).

249 Note that the humidity dependence mode and the expert mode can also be included in the valve sequencer
250 but are not used in a daily calibration routine.

251
252 A set of tools has been developed to quickly check daily calibration. In the field, analyzer and LHLG data
253 are archived daily and sent to the laboratory, i.e. at LSCE, Gif sur Yvette. They are checked semi-
254 automatically once a week to warn maintenance personnel in the event of a malfunction.

256 3- Performance of the instrument

257 The stability of the instrument has been tested over a large range of parameters. We show an example in
258 Table 2. We modified the air flow associated with standard A (the same results can be obtained with
259 standard B) between 200 and 400 sccm with an air flow on channel B of half the value of channel A. The
260 infusion rate was varied between 0.03 and 0.14 $\mu\text{L}/\text{min}$ in order to produce humidity levels of 400 and 800
261 ppmv. The 1σ standard deviations observed over 10 minutes plateaus are comparable to the standard
262 deviation obtained when the air flow is set to 300 sccm.

Air flow (sccm)	Infusion rate ($\mu\text{L}/\text{min}$)	Humidity (ppmv)	10 minutes 1σ standard deviation for humidity (ppmv)	$\delta^{18}\text{O}$ (‰)	10 minutes 1σ standard deviation for $\delta^{18}\text{O}$ (‰)
200	0.07	808	1	-7.88	0.89
300	0.11	851	2	-7.73	0.85
400	0.14	818	2	-7.95	0.90
200	0.03	374	1	-8.45	1.92
300	0.05	411	2	-9.16	1.64
400	0.07	415	3	-9.05	1.59

264
265 **Table 2 :** Evolution and stability of humidity and $\delta^{18}\text{O}$ (same water used for the different tests) for
266 different syringe infusion rates and dry air flows.

268 For routine measurement, air flow and infusion rate have been adjusted to optimize the stability of the
269 generated vapor while minimizing the dry air consumption. The LHLG is thus able to generate stable levels
270 of humidity (drift lower than 20 ppmv over one hour and 1σ below 10 ppmv over 10 minutes) from 70
271 ppmv to 2,400 ppmv following the optimal set-points shown in Table 3.

272

Humidity (ppmv)	Infusion rate ($\mu\text{L}/\text{min}$)	Dry Air flow (sccm)
80	0.01	300
160	0.02	300
320	0.04	300
800	0.1	300
1200	0.15	300
1600	0.2	300
2400	0.3	300

273

274 **Table 3:** Set-points for water infusion rate and dry air flow at a temperature of 20°C.

275

276 **3-1- No fractionation during water vaporization in the cavity**

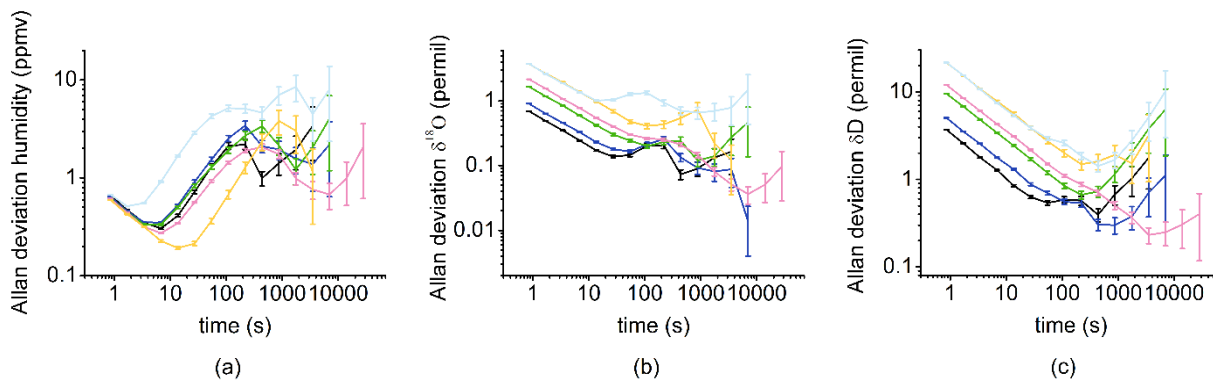
277 We have checked that there was no fractionation of the water during its transfer from the bottles to the
278 syringe pump, then from the syringe to the moist air generated in the vaporization chamber through the
279 following tests.

280 First, the isotopic composition of three different lab-standards calibrated against VSMOW at LSCE (H_2O -
281 CO_2 equilibration followed by IRMS for $\delta^{18}\text{O}$; Cavity RingDown Spectroscopy for δD ; calibrated every 3
282 years using VSMOW and VSLAP provided by IAEA) have been compared, after their generation by the
283 present LHLG and by the commercial SDM, both at a humidity of 2,000 ppmv over 50-min time spans. The
284 measured $\delta^{18}\text{O}$ and δD values agreed to within 0.5‰ and 2‰, respectively, for the 3 lab-standard waters
285 calibrated against VSMOW: EPB ($\delta^{18}\text{O} = -6.24$ ‰; $\delta\text{D} = -43.6$ ‰), NEEM ($\delta^{18}\text{O} = -33.50$ ‰; $\delta\text{D} = -257.2$ ‰),
286 FP5 ($\delta^{18}\text{O} = -48.33$ ‰; $\delta\text{D} = -383.5$ ‰). Second, the measured isotopic composition of the same standard
287 (FP5) generated at different humidity levels between 1,000 and 2,400 ppmv by the SDM and the LHLG
288 show the same $\delta^{18}\text{O}$ (δD) evolution with humidity within respective uncertainties (Supplementary Figure
289 S1).

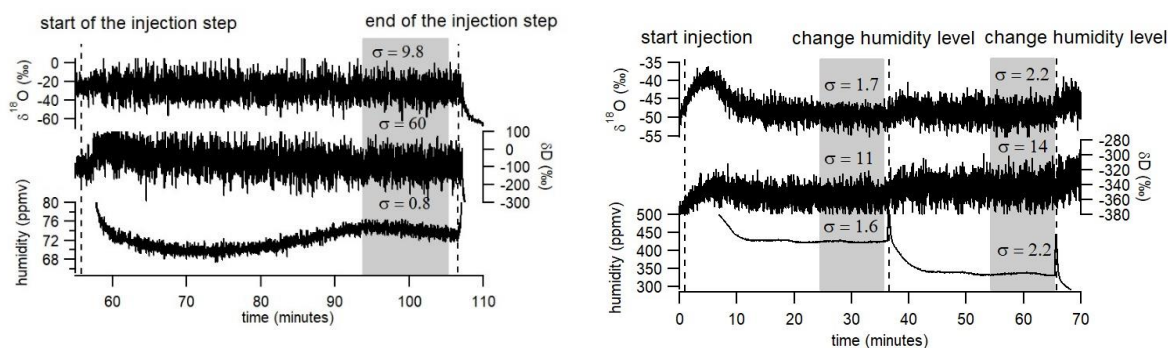
290

291 **3-2- Stability of the water vapor delivery and associated water isotopic composition**

292



293
 294 **Figure 3:** Allan deviation over 4 hours for different humidity levels (black 1,080 ppmv; dark blue 770 ppmv;
 295 green 400 ppmv; pink 320 ppmv; yellow and light blue 170 ppmv) for humidity (a), $\delta^{18}\text{O}$ (b) and δD (c).



296 **Figure 4:** Records of $\delta^{18}\text{O}$, δD and humidity over 3 humidity plateaus (72 ppmv on the left, 425 and 335
 297 ppmv on the right) obtained with the LHLG. The grey rectangles indicate the period (10 min) over which the
 298 average values are kept for calibrating the data generated by a L2130-i analyzer.

299
 300
 301 A proper approach to quantify the stability of our system is to use the Allan variance defined as:
 302

$$\sigma_y^2(t) = \frac{1}{2} \langle (y_{n+1} - y_n)^2 \rangle \quad (\text{eq. 3})$$

303
 304
 305 where y_n are the successive measurements over a period t .
 306 An Allan variance plot as a function of averaging time is indeed useful to determine the optimal time over
 307 which the sample humidity and the isotopic composition should be averaged to obtain a precise
 308 determination (low standard deviation) and avoid drift. Figure 3 displays the Allan deviation (square root
 309 of the Allan variance) in $\delta^{18}\text{O}$, δD and humidity obtained by running a long plateau of standard A or
 310 standard B in the “infuse” mode over 4 hours for different humidity levels. The humidity variance always
 311 stays below 10 ppmv over the 4 hours test and the $\delta^{18}\text{O}$ and δD Allan deviations display minimum values
 312 below 1 ‰ and 7 ‰ respectively. The minimum value for the $\delta^{18}\text{O}$ and δD Allan deviation is generally

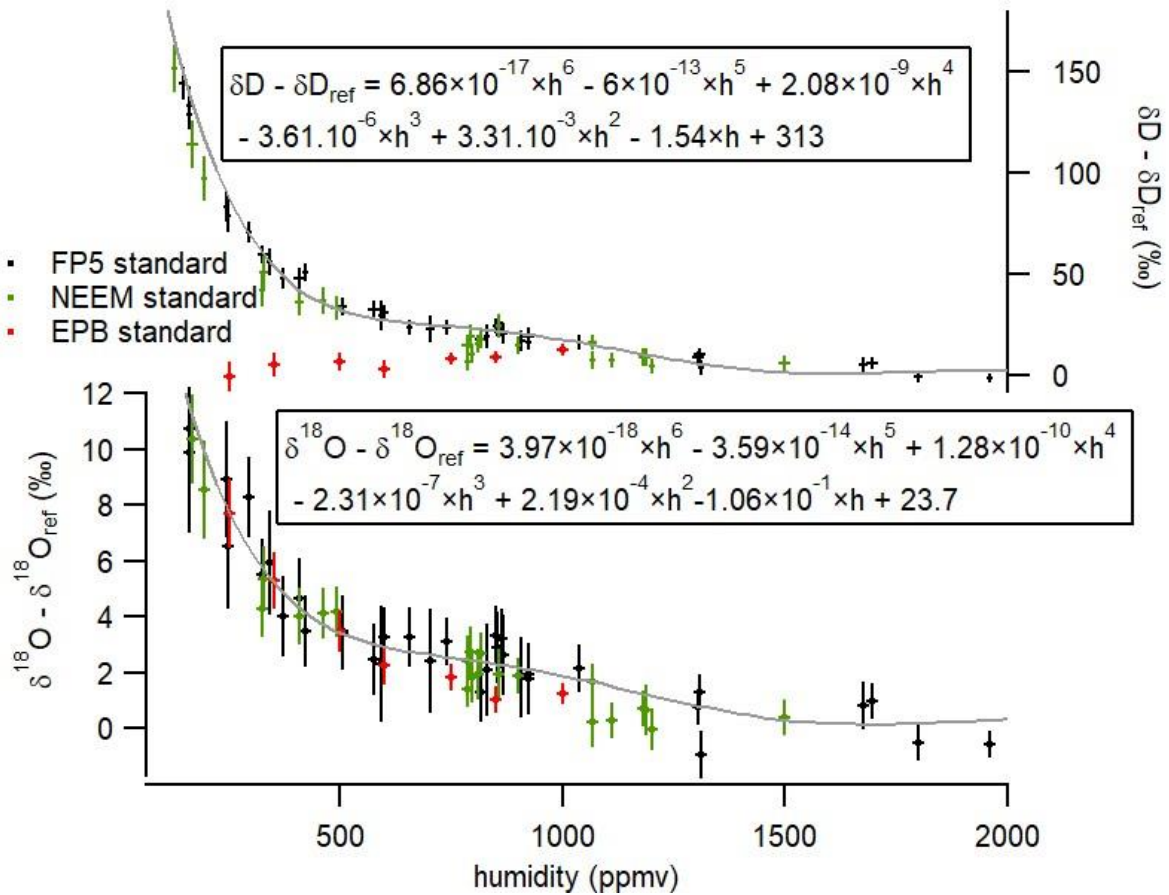
313 obtained for about 15 minutes of measurement. While the Allan deviation of $\delta^{18}\text{O}$ and δD is dependent on
314 the analyzer used, we observe that the Allan deviation at 1000 s (17 minutes) for $\delta^{18}\text{O}$ and δD also depends
315 to some extent on the humidity level: the lowest levels are obtained for humidity levels of 770-1,080 ppmv
316 and the highest levels are obtained for humidity level of 170 ppmv.

317 In the routine mode (Figure 4), we perform plateaus of 30 to 50 minutes (50 minutes when the instrument
318 is unattended since the time to reach the plateau varies between a few minutes to 30 minutes). We then
319 select the last 10 minutes before the following switch of the instrument to measure the average level of
320 humidity and the isotopic ratios, $\delta^{18}\text{O}$ and δD . We also calculate the associated standard deviations and
321 reject the values if the humidity standard deviation exceeds 30 ppmv over these last 10 minutes. In Figure
322 4, one observes that the standard deviations for humidities generated in the routine mode are actually
323 much lower. The corresponding standard deviations for the isotopic ratios ($\delta^{18}\text{O}$ and δD , see values
324 indicated in Figure 4) increase with decreasing humidity, reflecting the decrease of the molecular
325 absorption signal recorded by the L2130-i laser analyzers. This has an obvious impact on the determination
326 of the relationship between humidity and water vapor isotopic composition.

327 The performance of the present LHLG can be compared to the performance of the SDM (see
328 Supplementary Figures S1 and S2). First (Figure S2), a comparison has been performed at a humidity level
329 of 800 ppmv, for which we have numerous daily calibrations performed with a SDM from a 4.5 years field
330 deployment in Svalbard (Leroy-Dos Santos et al., 2020). The best SDM performance displays a standard
331 deviation 1σ of 31 ppmv, which is significantly worse than the performance of the LHLG (standard
332 deviation 1σ lower than 10 ppmv on average and down to 2 ppmv for 30% of the generated humidity
333 plateaus). Second (Figure S1), while we measure the same influence of humidity on measured $\delta^{18}\text{O}$ and δD
334 either with the SDM or with the LHLG, the 1σ values on humidity levels are much larger for the SDM than
335 for the LHLG.

336

337 **3-3- Determination of the influence of humidity on water vapor isotopic composition**



338
 339 **Figure 5:** Influence of humidity on the isotopic composition ($\delta^{18}\text{O}$ and δD) of the vapor obtained with the
 340 LHLG with 3 water lab-standards. The error bars are calculated as the standard deviation (1σ) over the
 341 generated values by the L2130-i instrument during 10 minutes at 1 second resolution (i.e. without any pre-
 342 averaging of the raw dataseries). The $\delta^{18}\text{O}_{\text{ref}}$ and $\delta\text{D}_{\text{ref}}$ are the values of the injected water standards at
 343 2,000 ppmv. The grey lines represent the polynomial fits for the influence of humidity on the water isotopic
 344 composition (equations 4 and 5 also written on the graph).

345
 346 Contrary to the commercial SDM, which hardly produces stable and reproducible humidity levels below
 347 500 ppmv, the LHLG was able to daily produce stable 10-minute humidity plateaus over the range from 70
 348 ppmv to 2,400 ppmv with an associated standard deviation of the order of 10 ppmv over more than one
 349 year at the Concordia and Dumont d'Urville stations (installation in December 2018). The stability of the
 350 LHLG allows a robust quantification of the L2130-i analyzer drift thanks to a daily measurement of the
 351 same water isotopic standard reference (see Table S2 showing actually no measurable drift over a 3-week
 352 period). It also permits the characterization of the measurement non-linearities observed at low-humidity
 353 (Figure 5). The more than one-year long Concordia and Dumont d'Urville datasets showed that the
 354 humidity dependence of $\delta^{18}\text{O}$ and δD did not vary measurably. The uncertainty of the obtained calibration

355 curve can be attributed entirely to the L2130-i $\delta^{18}\text{O}$ and δD measurements. In other words, the uncertainty
 356 bars in the horizontal (x-) axis in Figure 5, associated with the LHLG, are negligible.

357 Our data show a result already observed in Weng et al. (2020): while the dependency of $\delta^{18}\text{O}$ and δD to
 358 humidity is similar for low $\delta^{18}\text{O}$ and δD lab-standards (NEEM and FP5), we observe a different behavior for
 359 the δD vs humidity relationship for the high $\delta^{18}\text{O}$ and δD lab-standard EPB. This result strengthens the
 360 recommendation of Weng et al. (2020) to use two water standards in the range of the measured water
 361 vapor isotopic composition to best calibrate our final data. In our case, our applications were in Antarctica,
 362 so that we used our two lowest lab-standards (NEEM and FP5). For the two standards and for this particular
 363 Picarro L2130-i (results are expected to depend on the instrument), the same dependency of isotopic
 364 composition vs humidity is observed. We express this dependency as the relationship between the
 365 difference in δD or $\delta^{18}\text{O}$ between the measured value at the given humidity and the value of the same
 366 standard measured at a humidity of 2,000 ppmv. The experimental data for NEEM and FP5 from Figure 5
 367 are fitted through polynomial functions with respect to humidity h (in ppmv):

368
 369
$$\delta^{18}\text{O} - \delta^{18}\text{O}_{\text{ref}} = 3.97 \times 10^{-18} \times h^6 - 3.586315 \times 10^{-14} \times h^5 + 1.2843645994 \times 10^{-10} \times h^4 - 2.3087753445094 \times 10^{-7} \times h^3$$

 370
$$+ 2.1857285350473100 \times 10^{-4} \times h^2 - 0.10603325432255400000 \times h + 23.7 \text{ (eq. 4)}$$

371
 372
$$\delta\text{D} - \delta\text{D}_{\text{ref}} = 6.859 \times 10^{-17} \times h^6 - 6.0047709 \times 10^{-13} \times h^5 + 2.0790331349 \times 10^{-9} \times h^4 - 3.61319302207374 \times 10^{-6} \times h^3$$

 373
$$+ 3.30716141498371 \times 10^{-3} \times h^2 - 1.53651645114701 \times h + 313 \text{ (eq. 5)}$$

 374

375 These curves are valid only for a given Picarro analyzer and for humidity higher than 70 ppmv and lower
 376 than 2,000 ppmv. Outside this calibration range, the extrapolation of the polynomial function may lead to
 377 anomalous corrections.

378
 379 After this correction, the measured values corrected from humidity dependence are corrected using the
 380 comparison of the measured values of the 2 standards at 2,000 ppmv to their VSMOW calibrated values
 381 as explained in section 3.5 below.

382
 383 **3.5- Accuracy of the system and calibration on the VSMOW-VSLAP scale**

384 The accuracy of the system has been addressed performing a 2-standard calibration and measuring a third
 385 standard treated as an unknown. We used two lab-standards calibrated vs VSMOW on the VSMOW-VSLAP
 386 scale with large $\delta^{18}\text{O}$ and δD differences (EPB and FP5) and used the lab-standard NEEM, also
 387 independently calibrated against VSMOW. The 3 lab-standards have been vaporized at 800 ppmv and
 388 measured by the same L2130-i analyzer.

389

Standard	VSMOW calibrated value	Measured value at 800 ppmv	Measured value corrected from
----------	------------------------	----------------------------	-------------------------------

			humidity dependence (Equation 1)
EPB	-6.24 ‰	-8.27 ‰	-10.78 ‰
NEEM	-33.5 ‰	-34.48 ‰	-36.99 ‰
FP5	-48.33 ‰	-49.02 ‰	-51.53 ‰

390

391 **Table 4:** Comparison of measured vs VSMOW calibrated $\delta^{18}\text{O}$ values for 3 standards measured with a
392 Picarro analyzer after generation of water vapor using the LHLG.

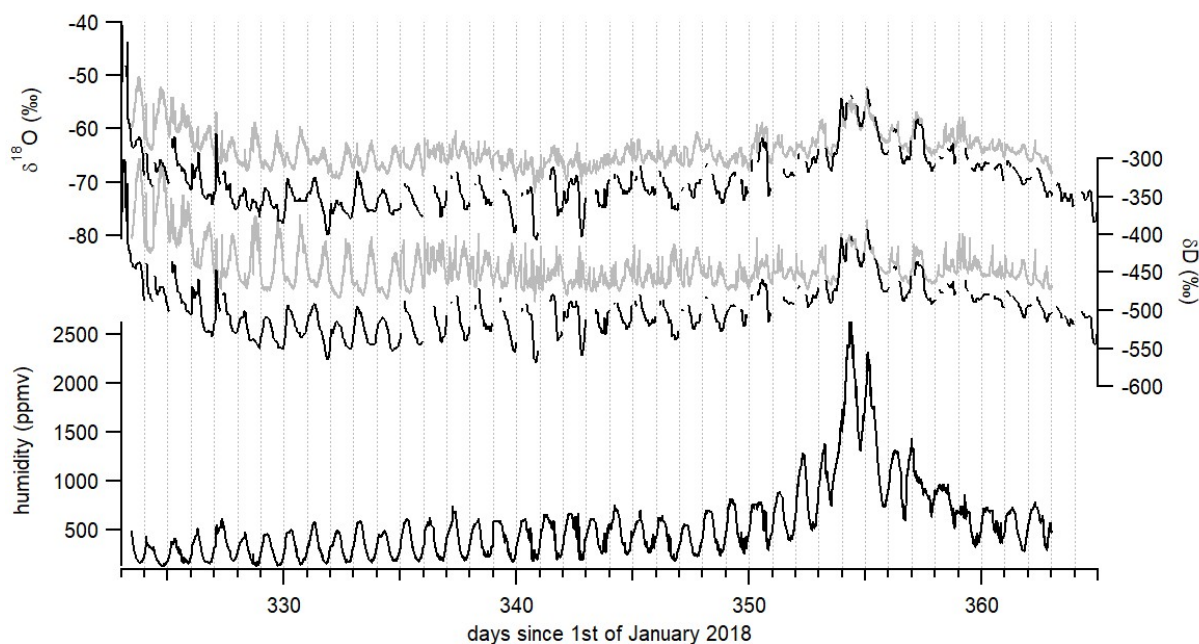
393

394 We used the measured and true values of EPB and FP5 to estimate the $\delta^{18}\text{O}$ value of the NEEM standard
395 from its measured value (Table 4). Using the linear relationship obtained from VSMOW calibrated EPB
396 and FP5 $\delta^{18}\text{O}$ vs measured EPB and FP5 $\delta^{18}\text{O}$ values (Figure S3) following the recommendations of the
397 National Institute of Standards and Technology (NIST, reference material 8535a) leads to an estimated
398 NEEM $\delta^{18}\text{O}$ of -33.31 ‰ to be compared to the independently VSMOW calibrated value of -33.5 ‰.
399 Given the uncertainty of about 0.8-1 ‰ when measuring $\delta^{18}\text{O}$ around 800 ppmv, we can conclude that
400 the system is accurate.

401

402 **4- Application**

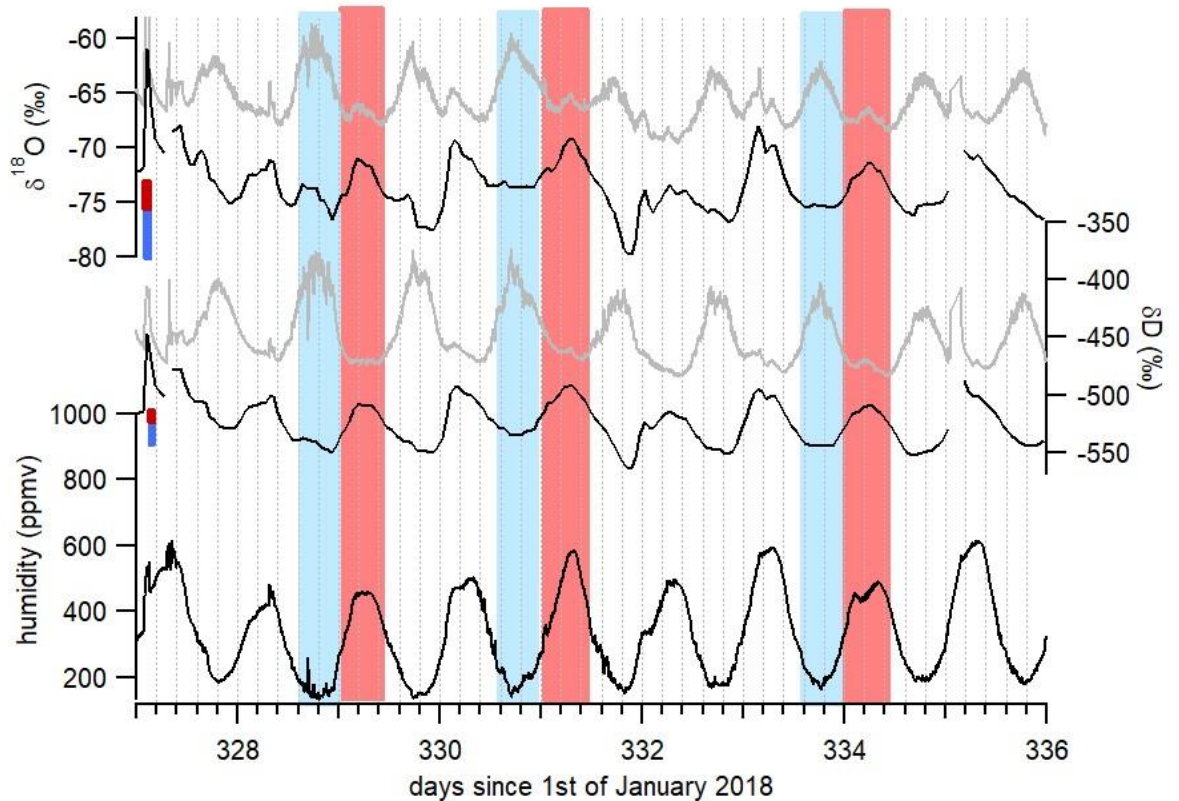
403 The main application of this device is the interpretation of water isotopic profiles at dry sites, in particular
404 in polar regions. As shown in Figure 5, the influence of humidity on the measurement of the water vapor
405 isotopic composition with the L2130-i analyzer is large when humidity is below 1,000 ppm and increases
406 when humidity decreases. Even though the precise isotope ratio-humidity calibration curve is likely to be
407 different from one analyzer to another, all laser-based water isotope analyzers investigated to date have
408 shown a strongly non-linear response at low-humidity levels (Guilpart et al., 2017; Leroy Dos-Santos, 2020;
409 Weng et al., 2020). At the Concordia station, even in summer, humidity is generally below 1,000 ppmv
410 (Figure 6) so that the interpretation of the diurnal variability of the water vapor isotopic composition is
411 strongly affected by the dependency of the measured $\delta^{18}\text{O}$ and δD signals on humidity. Figure 6 displays
412 such diurnal variabilities during austral summer 2018-2019 at Concordia and the consequently large
413 correction of the isotopic records (uncorrected in grey and corrected in black).



414
 415 **Figure 6:** $\delta^{18}\text{O}$, δD and humidity records over December 2018 and beginning of January 2019. Raw isotopic
 416 values are in grey. Corrected isotopic values at hourly resolution are in black after correction of the
 417 influence of humidity on the water isotopic ratios and adjustment of $\delta^{18}\text{O}$ and δD values on the VSMOW-
 418 VSLAP scale using relationships between measured lab-standard values and known VSMOW calibrated lab-
 419 standard values.

420
 421 The data clearly demonstrate the importance of the humidity correction which shifts the curves generally
 422 to lower isotopic ratio values. However, the difference between uncorrected and corrected data is
 423 particularly important in the observation of the diurnal variability, illustrated even better when zooming
 424 in on a section of the data, as in Figure 7. When looking in detail at the diurnal variability in the raw $\delta^{18}\text{O}$
 425 and δD isotope data, some periods stand out with two identified daily peaks, one in phase with the
 426 humidity peak (marked in red in Figure 7) and one occurring during the period of minimum humidity
 427 (marked in blue in Figure 7). The strong non-linearity of the calibration curve of Figure 5 suggests that
 428 artificial peaks in $\delta^{18}\text{O}$ and δD could be due to changing humidity levels. Indeed, after correcting the data
 429 for the humidity dependence of the analyzer (black curve in Figure 7), the isotopic peaks occurring during
 430 humidity minima are diminished or disappear altogether, while the peaks occurring during humidity
 431 maxima are amplified. More strikingly, the phase of the signal changes by practically 180° over some
 432 periods. Whereas the raw isotope signal peaks during the night, the corrected record shows higher isotope
 433 ratios during daytime. The diurnal variability recorded on both raw and corrected isotopic values during a
 434 period with higher humidity level, hence when the isotope ratio-humidity correction is smaller (around
 435 day 355 in figure 6), also shows that the $\delta^{18}\text{O}$ (δD) diurnal cycles are indeed in-phase with the humidity
 436 cycle. This result confirms the correlation between humidity cycles and $\delta^{18}\text{O}$ and δD of the water vapor at

437 the daily scale at Concordia as reported by Casado et al. (2016). We thus conclude that the anticorrelation
 438 observed between $\delta^{18}\text{O}$ (δD) and humidity in the raw data (highlighted in blue in Figure 7) during periods
 439 of low-humidity is an artefact due to the influence of the humidity level on the vapor isotopic
 440 measurements by the L2130-i analyzer.



441
 442 **Figure 7:** Focus on diurnal variability of $\delta^{18}\text{O}$, δD and humidity recorded at Concordia. Grey curves show the
 443 raw measurements and black curves the corrected records. The red (blue) bars indicate the calculated
 444 uncertainty due to the isotopic ratio vs humidity dependence (Figure 5) on the corrected $\delta^{18}\text{O}$ and δD values
 445 during periods with maximum (minimum) humidity. The red (blue) rectangles indicate half day with
 446 maximum (minimum) humidity.

447
 448 **5- Conclusion**

449 We have developed an autonomous instrument for low-humidity generation (70 to 2,400 ppmv) with
 450 controlled water vapor isotopic composition specifically aimed at carrying out continuous measurements
 451 of the water vapor isotopic composition using a laser-based spectrometer in regions characterized by very
 452 low-humidity, such as polar regions. If needed, an interface permits to conveniently connect the new LHLG
 453 to the valve sequencer port of commercial Picarro instruments. After more than one year of routine
 454 operation on two Antarctic sites (Dumont d'Urville and Concordia), this instrument has proven to be very
 455 reliable and robust. It consistently generates stable humidity levels with a 1σ variability lower than 10

456 ppmv over more than 10 minutes. Besides, its performance is significantly better than that of the Picarro
457 SDM at low humidity.

458 We used this instrument for the calibration of our water isotopic data with a special focus on accurately
459 quantifying the influence of humidity on the measured isotopic composition of the water vapor. This effect
460 is huge at low-humidity. We showed that this has an important impact on the interpretation of the diurnal
461 cycles of $\delta^{18}\text{O}$ and δD in the water vapor at the Concordia station at humidity below 1,500 ppmv. We were
462 able to confirm that, at this site, the diurnal $\delta^{18}\text{O}$ and δD variability is actually correlated with humidity
463 variability, which would not have been possible without the new LHLG instrument.

464 Finally, the development of such an instrument is an important step forward to a better understanding of
465 the transfer function between climate parameters and the isotopic composition of deep ice cores from
466 the remote East Antarctic plateau, especially in the context of the new program “Beyond EPICA”. It should
467 be completed by ongoing development of laser spectrometers better adapted to low-humidity levels, such
468 as those based on the technique of Optical Feedback Cavity Enhanced Absorption Spectroscopy (OFCEAS)
469 (Casado et al., 2016; Landsberg, 2014; Landsberg et al., 2014).

470

471 **Code availability**

472 The software (HumGen) can be downloaded on line (<https://github.com/ojsd/humgen>;
473 <https://doi.org/10.5281/zenodo.4003465>).

474

475 **Competing interests**

476 The authors declare that they do not have any competing interest.

477

478 **Author contributions**

479 CLDS, MC, FP and EK designed and built the instrument. OJ realized the software interface development.
480 CLDS, MC and AL installed the instrument in Antarctica and tested it extensively. EK, SK, MF, AL and EF
481 tested the instrument in the laboratory. AL wrote the manuscript with the help of all co-authors.

482

483 **Acknowledgments**

484 The development presented in this manuscript is largely inspired from the initial PhD work of Janek
485 Landsberg which we gratefully acknowledge here. The research leading to these results has received
486 funding from the Antarctic Snow program of the Fondation Prince Albert II de Monaco, the ANR EAIIST and
487 CNRS-LEFE program ADELISE. The deployment of this instrument in the field was made possible through
488 the logistic support of the NIVO2 & ADELISE IPEV programs. We thank the two reviewers for their useful
489 comments which greatly improved the manuscript.

490

491 **References**

- 492 Aemisegger, F., Sturm, P., Graf, P., Sodemann, H., Pfahl, S., Knohl, A. and Wernli, H.: Measuring variations
493 $\delta^{18}\text{O}$ and $\delta^2\text{H}$ in atmospheric water vapour using two commercial laser-based spectrometers: an
494 instrument characterisation study, *Atmos. Meas. Tech.*, 5(7), 1491–1511, doi:10.5194/amt-5-1491-2012,
495 2012.
- 496 Bailey, H. L., Kaufman, D. S., Henderson, A. C. G. and Leng, M. J.: Synoptic scale controls on the $\delta^{18}\text{O}$ in
497 precipitation across Beringia, *Geophys. Res. Lett.*, 42(11), 4608–4616, doi:10.1002/2015GL063983, 2015.
- 498 Bastrikov, V., Steen-Larsen, H. C., Masson-Delmotte, V., Griбанov, K., Cattani, O., Jouzel, J. and Zakharov,
499 V.: Continuous measurements of atmospheric water vapour isotopes in western Siberia (Kourovka),
500 *Atmos. Meas. Tech.*, 7(6), 1763–1776, doi:10.5194/amt-7-1763-2014, 2014.
- 501 Bonne, J.-L., Masson-Delmotte, V., Cattani, O., Delmotte, M., Risi, C., Sodemann, H. and Steen-Larsen, H.
502 C.: The isotopic composition of water vapour and precipitation in Ivittuut, southern Greenland, *Atmos.*
503 *Chem. Phys.*, 14(9), 4419–4439, doi:10.5194/acp-14-4419-2014, 2014.
- 504 Bréant, C., Leroy Dos Santos, C., Agosta, C., Casado, M., Fourré, E., Goursaud, S., Masson-Delmotte, V.,
505 Favier, V., Cattani, O., Prié, F., Golly, B., Orsi, A., Martinerie, P. and Landais, A.: Coastal water vapor isotopic
506 composition driven by katabatic wind variability in summer at Dumont d’Urville, coastal East Antarctica,
507 *Earth Planet. Sci. Lett.*, 514, 37–47, doi:10.1016/j.epsl.2019.03.004, 2019.
- 508 Casado, M., Landais, A., Masson-Delmotte, V., Genthon, C., Kerstel, E., Kassi, S., Arnaud, L., Picard, G., Prie,
509 F., Cattani, O., Steen-Larsen, H.-C., Vignon, E. and Cermak, P.: Continuous measurements of isotopic
510 composition of water vapour on the East Antarctic Plateau, *Atmos. Chem. Phys. Discuss.*, 1–26,
511 doi:10.5194/acp-2016-8, 2016.
- 512 Casado, M., Landais, A., Picard, G., Münch, T., Laepple, T., Stenni, B., Dreossi, G., Ekaykin, A., Arnaud, L.,
513 Genthon, C., Touzeau, A., Masson-Delmotte, V. and Jouzel, J.: Archival processes of the water stable
514 isotope signal in East Antarctic ice cores, *Cryosphere*, 12(5), doi:10.5194/tc-12-1745-2018, 2018.
- 515 Dong, F. and Baer, D. Development and Deployment of a Portable Water Isotope Analyzer for Accurate,
516 Continuous and High-Frequency Oxygen and Hydrogen Isotope Measurements in Water Vapor and Liquid
517 Water, in *Geophysical Research Abstracts*, 12:EGU2010-5571, 2010.
- 518 Ellehoj, M. D., Steen-Larsen, H. C., Johnsen, S. J. and Madsen, M. B.: Ice-vapor equilibrium fractionation
519 factor of hydrogen and oxygen isotopes: Experimental investigations and implications for stable water
520 isotope studies, *Rapid Commun. Mass Spectrom.*, 27(19), 2149–2158, doi:10.1002/rcm.6668, 2013.
- 521 Genthon, C., Piard, L., Vignon, E., Madeleine, J.-B., Casado, M. and Gallée, H.: Atmospheric moisture
522 supersaturation in the near-surface atmosphere at Dome C, Antarctic Plateau, *Atmos. Chem. Phys.*, 17(1),
523 691–704, doi:10.5194/acp-17-691-2017, 2017.
- 524 Gkinis, V., Popp, T. J., Johnsen, S. J. and Blunier, T.: A continuous stream flash evaporator for the calibration
525 of an IR cavity ring-down spectrometer for the isotopic analysis of water, *Isotopes Environ. Health Stud.*,
526 46(4), 463–475, doi:10.1080/10256016.2010.538052, 2010.
- 527 Guilpart, E., Vimeux, F., Evan, S., Brioude, J., Metzger, J., Barthe, C., Risi, C. and Cattani, O.: The isotopic
528 composition of near-surface water vapor at the Maïdo observatory (Reunion Island, southwestern Indian
529 Ocean) documents the controls of the humidity of the subtropical troposphere, *J. Geophys. Res. Atmos.*,
530 122(18), 9628–9650, doi:10.1002/2017JD026791, 2017.

531 Iannone, R., Romanini, D., Kassi, S., Meijer, H. A. J. and Kerstel, E.: A Microdrop Generator for the
532 Calibration of a Water Vapor Isotope Ratio Spectrometer, *J. Atmos. Ocean. Technol.*, 26,
533 doi:10.1175/2008JTECHA1218.1, 2009.

534 Jouzel, J., Masson-Delmotte, V., Cattani, O., Dreyfus, G., Falourd, S., Hoffmann, G., Minster, B., Nouet, J.,
535 Barnola, J. M., Chappellaz, J., Fischer, H., Gallet, J. C., Johnsen, S., Leuenberger, M., Loulergue, L., Luethi,
536 D., Oerter, H., Parrenin, F., Raisbeck, G., Raynaud, D., Schilt, a, Schwander, J., Selmo, E., Souchez, R.,
537 Spahni, R., Stauffer, B., Steffensen, J. P., Stenni, B., Stocker, T. F., Tison, J. L., Werner, M. and Wolff, E. W.:
538 Orbital and millennial Antarctic climate variability over the past 800,000 years., *Science*, 317(5839), 793–
539 796, doi:10.1126/science.1141038, 2007.

540 Kerstel, E. Modeling the Dynamic Behavior of a Droplet Evaporation Device for the Delivery of Isotopically
541 Calibrated Low-Humidity Water Vapor, *Atmospheric Measurement Techniques Discussions*, 1–19.
542 <https://doi.org/10.5194/amt-2020-428>, 2020.

543 Kopec, B., Lauder, A., Posmentier, E. and Feng, X.: The diel cycle of water vapor in west Greenland, *J.*
544 *Geophys. Res. Atmos.*, 119(15), 9386–9399, 2014.

545 Landsberg, J.: Développement d'un spectromètre laser OF-CEAS pour les mesures des isotopes de la
546 vapeur d'eau aux concentrations de l'eau basses. [online] Available from:
547 <http://www.theses.fr/2014GRENY052/document>, 2014.

548 Landsberg, J., Romanini, D. and Kerstel, E.: Very high finesse optical-feedback cavity-enhanced absorption
549 spectrometer for low concentration water vapor isotope analyses., *Opt. Lett.*, 39(7), 1795–1798,
550 doi:10.1364/OL.39.001795, 2014.

551 Lee, X., Sargent, S., Smith, R. and Tanner, B.: In Situ Measurement of the Water Vapor $^{18}\text{O}/^{16}\text{O}$ Isotope
552 Ratio for Atmospheric and Ecological Applications, *J. Atmos. Ocean. Technol.*, 22(5), 555–565,
553 doi:10.1175/JTECH1719.1, 2005.

554 Leroy Dos Santos, C., Masson-Delmotte, V., Casado, M., Fourré, E., Steen-Larsen, H-C, Maturilli, M., Orsi,
555 A., Berchet, A., Cattani, O., Minster, B., Gherardi, J. and Landais, A., A 4.5 year-long record of Svalbard
556 water vapor isotopic composition documents winter air mass origin, *J. Geophys. Research*, 125 (23),
557 (10.1029/2020JD032681), 2020.

558 Ritter, F., Steen-larsen, H. C., Werner, M., Masson-Delmotte, V., Orsi, A., Behrens, M., Birnbaum, G.,
559 Freitag, J., Risi, C. and Kipfstuhl, S.: Isotopic exchange on the diurnal scale between near-surface snow and
560 lower atmospheric water vapor at Kohnen station , East Antarctica, *J. Geophys. Research* (February), 1–
561 35, doi:10.5194/tc-2016-4, 2016.

562 Sayres, David S, E J Moyer, T F Hanisco, J M St Clair, F N Keutsch, A O'Brien, N T Allen, et al., A New Cavity
563 Based Absorption Instrument for Detection of Water Isotopologues in the Upper Troposphere and Lower
564 Stratosphere. *Review of Scientific Instruments* 80 (4): 44102–14.
565 <http://link.aip.org/link/?RSI/80/044102/1>, 2009.

566 Schmidt, M., Maseyk, K., Lett, C., Biron, P., Richard, P., Bariac, T. and Seibt, U.: Concentration effects on
567 laser-based $\delta^{18}\text{O}$ and $\delta^2\text{H}$ measurements and implications for the calibration of vapour measurements with
568 liquid standards, *Rapid Commun. Mass Spectrom.*, 24(24), 3553–3561, doi:10.1002/rcm.4813, 2010.

569 Sodemann, H., Aemisegger, F., Pfahl, S., Bitter, M., Corsmeier, U., Feuerle, T., Graf, P., Hankers, R., Hsiao,
570 G., Schulz, H., Wieser, A. and Wernli, H.: The stable isotopic composition of water vapour above Corsica
571 during the HyMeX SOP1 campaign: Insight into vertical mixing processes from lower-tropospheric survey
572 flights, *Atmos. Chem. Phys.*, 17(9), 6125–6151, doi:10.5194/acp-17-6125-2017, 2017.

573 Steen-Larsen, H. C., Masson-Delmotte, V., Hirabayashi, M., Winkler, R., Satow, K., Prié, F., Bayou, N., Brun,
574 E., Cuffey, K. M., Dahl-Jensen, D., Dumont, M., Guillevic, M., Kipfstuhl, S., Landais, A., Popp, T., Risi, C.,
575 Steffen, K., Stenni, B. and Sveinbjörnsdóttir, A. E.: What controls the isotopic composition of Greenland
576 surface snow?, *Clim. Past*, 10(1), 377–392, doi:10.5194/cp-10-377-2014, 2014.

577 Sturm, P. and Knohl, A.: Water vapor $\delta^2\text{H}$ and $\delta^{18}\text{O}$ measurements using off-axis integrated cavity output
578 spectroscopy, *Atmos. Meas. Tech. Discuss.*, 2(4), 2055–2085, doi:10.5194/amtd-2-2055-2009, 2009.

579 Tremoy, G., Vimeux, F., Cattani, O., Mayaki, S., Souley, I. and Favreau, G.: Measurements of water vapor
580 isotope ratios with wavelength-scanned cavity ring-down spectroscopy technology: new insights and
581 important caveats for deuterium excess measurements in tropical areas in comparison with isotope-ratio
582 mass spectrometry, *Rapid Commun. Mass Spectrom.*, 25(23), 3469–3480, doi:10.1002/rcm.5252, 2011.

583 Wang, L., Caylor, K. and Dragoni, D.: On the calibration of continuous, high-precision $\delta^{18}\text{O}$ and $\delta^2\text{H}$
584 measurements using an off-axis integrated cavity output spectrometer, *Rapid Commun. Mass Spectrom.*,
585 23, 530–536, doi:10.1002/rcm.3905, 2009.

586 Weng, Y., Touzeau, A. and Sodemann, H.: Impact of isotope composition on the humidity dependency
587 correction of water vapour isotope measurements with infra-red cavity ring-down spectrometers, *Atmos.*
588 *Meas. Tech.*, 13, 3167–3190, <https://doi.org/10.5194/amt-13-3167-2020>, 2020.

589

590

591

592